Spectral broadening and pulse shaping in the deep ultraviolet

JULIA CODERE[1], BRETT J PEARSON[2], BRIAN KAUFMAN[3], LOC THI-HOANG NGO[1], MARTIN G COHEN[1], MATTHEW BAIN[3], THOMAS WEINACHT[1,5], AND RUARIDH FORBES[3,4,*]

[1] Department of Physics and Astronomy, Stony Brook University, Stony Brook, NY 11794, USA
[2] Department of Physics and Astronomy, Dickinson College, Carlisle, PA 17013, USA
[3] Linac Coherent Light Source, SLAC National Accelerator Laboratory, Menlo Park, CA 94025, USA
[4] Department of Chemistry, University of California, Davis, One Shields Ave, Davis, CA 95616, USA
[5] thomas.weinacht@stonybrook.edu
[*] ruforbes@ucdavis.edu

Compiled January 9, 2026

We report the generation and shaping of ∼20 femtosecond pulses in the deep ultraviolet (DUV). Our approach combines spectral broadening in a stretched hollow-core fiber with compression and shaping via an acousto-optic modulator-based pulse shaper. The pulse shaper allows for automatic compression, useful for in-air delivery of pulses to two-dimensional (2D) spectroscopy and other time-resolved experiments. Unlike previous DUV pulse generation schemes that lack phase stability, our method enables programmable generation of phase-locked pulse pairs with attosecond-level stability. We demonstrate pulse characterization via self-diffraction frequency-resolved optical gating and dispersion scan methods in the DUV and validate performance through a pump-probe experiment resolving electronic dynamics on attosecond timescales.

http://dx.doi.org/10.1364/ao.XX.XXXXXX

Ultrafast pulses in the deep ultraviolet (DUV) region are of significant interest for probing and controlling electronic dynamics in molecules because they can directly drive valence excitations in neutral species [1] without ionizing, as is typically the case with extreme ultraviolet pulses [2, 3]. Such capabilities are particularly valuable in time-resolved spectroscopy, where access to electronic transitions in the DUV enables tracking of excited-state dynamics. However, the generation of ultrashort pulses in the DUV presents multiple challenges.

First, there are no available gain media that can directly produce few-cycle laser pulses in the DUV, necessitating the use of nonlinear upconversion techniques to reach these wavelengths. These methods, such as harmonic generation, inevitably face a trade-off between efficiency and bandwidth, especially at shorter wavelengths where nonlinear conversion becomes less efficient [4]. Moreover, compressing the broad spectral bandwidth required for ∼ 20 fs pulses in the DUV is technically demanding due to the limited availability of optical components. In particular, conventional chirped mirrors are inefficient/ineffective in this spectral range, and prism compressors cannot simultaneously compensate for both group velocity dispersion (GVD) and higher-order dispersion [5–7]. Pulse shaping provides a possible avenue for compression, and previous work has successfully used pulse shapers to compress supercontinuum light (e.g., see [8–10].

While DUV pulses as short as 3–8 fs have been demonstrated via cross-phase modulation [11] or resonant dispersive wave (RDW) emission [12] in gas-filled hollow-core fibers (HCFs), such pulses often require propagation in vacuum to avoid absorption or broadening in air or transmissive optics, complicating both pulse characterization and delivery to experimental targets [13, 14]. However, despite these constraints, recent efforts have exploited these DUV ultrafast sources in conventional laboratory environments [1, 15].

In this work, we demonstrate an efficient method for the generation, compression, and shaping of ultrashort DUV pulses. Our approach combines spectral broadening in a stretched, hollow-core fiber (S-HCF) with an acousto-optic modulator (AOM)-based pulse shaper, enabling compression to $<$ 20 fs durations. This builds on our recent successes in pulse compression and shaping in the visible [16] and infrared [17] spectral regions. The use of a programmable AOM also offers additional advantages, including real-time pulse characterization and high precision, flexible shaping capabilities that are essential for multidimensional spectroscopies [18, 19]. The programmability of the AOM also allows for pre-compensation of dispersion, enabling convenient propagation to experiments through air and windows.

The experimental arrangement is shown in panel (a) of Fig. 1. We start with a ytterbium (Yb) laser (Light Conversion Pharos) which has a central wavelength of 1025 nm and full-width at half-maximum (FWHM) pulse duration of 255 fs. Using sequential frequency doubling in two beta barium borate (BBO) crystals that are 1 mm and 500 μm thick, successively, we generate the fourth harmonic of the Yb laser. The pulse energy at the fundamental is 400 μJ, with up to 70 μJ converted to the fourth harmonic at a central wavelength of 256 nm; the spectrum after the crystals supports a FWHM 135 fs transform-limited pulse duration. Broadening of the DUV pulses is done via Kerr-induced

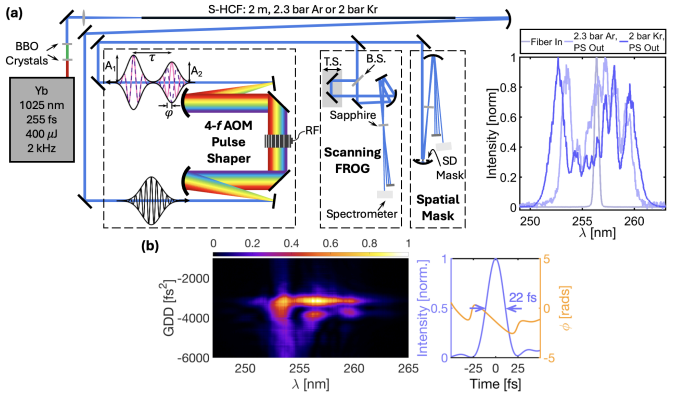

Fig. 1. Apparatus for generating, shaping, and characterizing broadband pulses in the DUV. **Panel (a):** The fourth harmonic of the Yb laser is generated using two BBO crystals, broadened in a S-HCF, and shaped in an AOM-based pulse shaper. The pulse is then characterized with either the scanning interferometer or spatial mask setup, both of which utilize self-diffraction (SD) as the nonlinearity. Also in panel (a) are measured spectra of the fiber input and pulse shaper output for 2.3 bar Ar and 2 bar Kr. **Panel (b):** shows an example of an SD-based d-scan done with the spatial mask (left) and the corresponding reconstructed pulse and phase (right), with the FWHM corresponding to a 22 fs pulse.

self-phase modulation with a 2 m long, 200 μm diameter S-HCF that is filled with monatomic gas. We can operate in a high or low energy mode, depending on the gas we choose to use. For typical experiments, the fiber is filled with either ∼2.3 bar of argon with 70 μJ input pulses or ∼2 bar of krypton with 20 μJ input pulses. In comparison to a theoretical limit for a Gaussian beam of 88%, we achieve throughputs of >50%, where the losses are due to absorption in the gas and degradation of the windows from UV exposure. Example spectra for the fiber input and pulse shaper output are shown in panel (b) of Fig. 1. The spectral bandwidths support FWHM pulse durations of 20 fs using argon and 18 fs using krypton.

An AOM-based, 4-f pulse shaper [20, 21] allows for both compression and characterization of the DUV pulses and builds on our previous work in the ultraviolet [22]. The shaper is setup as a zero-dispersion stretcher in a 4-f geometry, with an AOM placed at the Fourier plane. We utilize a matched pair of gratings with a groove density of 1200 lines/mm (∼ 75% first-order diffraction efficiency) and dielectric curved mirrors (Optoman) with a focal length of 1 m. This combination is such that the spectral beam spread at the Fourier plane fills the 36 mm AOM aperture while minimizing the ellipticity of the diffracted beam [23]. The acoustic wave in the AOM is generated by a radio frequency voltage from a computer-controlled arbitrary waveform generator (Chase Scientific) that allows shot-to-shot updating of the pulse up to a 50 kHz repetition rate [17]. The RF bandwidth is 100 MHz at a central frequency of 210 MHz. The fused silica AOM (Brimrose) achieves a first-order diffraction efficiency of ∼ 50%, yielding an overall pulse-shaper efficiency of ∼ 25%. These efficiencies degrade slowly with exposure of the optics to the UV light as a result of color center formation in the transmissive optics [24]. In the experimental results reported below [25] at 2 kHz repetition rate, we made use of ∼ 2 − 3 μJ, but the output of the pulse shaper can exceed 5 μJ when using argon gas in the fiber.[1]

As noted, degradation of transmissive optics is an issue in the DUV. Indeed, after a few months of using a previous AOM, we observed diffracted light even when there was no acoustic wave present. Inspection of the crystal under a microscope revealed a damage pattern with a 40 μm period, which matches the central wavelength of the acoustic wave inside the AOM. This damage is likely due to constructive interference of the undiffracted and diffracted DUV beams imprinting a permanent diffraction pattern within the AOM. To extend the lifetime of the current AOM, we randomize the overall phase of the acoustic wave for each laser shot. While having no effect on the optically shaped pulse, physically, this randomizes the locations of constructive interference between the undiffracted and diffracted DUV beams and prevents such patterned damage from reoccurring.

The output of the shaper is sent into an apparatus that includes two options for pulse characterization, one utilizing a scanning interferometer and the other a spatial mask (Fig. 1 panel (b)). Both options use self-diffraction (SD), a third-order nonlinear effect, generated in a 250 μm thick sapphire crystal, since second-harmonic generation is not viable in the DUV. In each approach, the pulse is split and focused into the nonlinear medium. The scanning interferometer is an amplitude-splitting approach that utilizes a beam-splitter to create the two arms of the interferometer. The spatial mask is a wavefront-splitting approach where the mode is spatially split with a 3D printed two-aperture mask placed directly in front of a focusing mirror such that the two sub-beams cross in the nonlinear medium. Both options have the capability to characterize the pulses via dispersion scan (d-scan) [26, 27] or frequency-resolved, optical gating (FROG) [28] with the assistance of the pulse shaper.

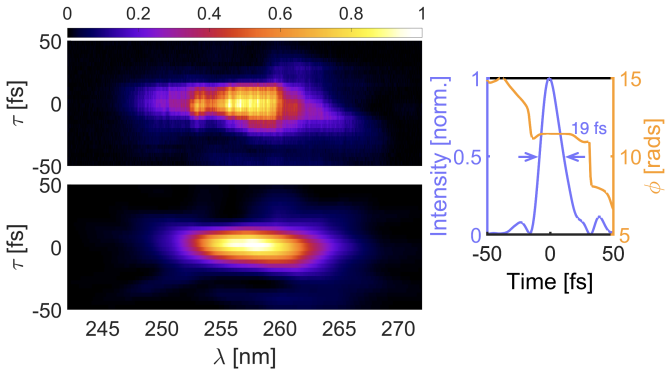

Fig. 2. Scanning SD-FROG for a 19 fs transform-limited pulse (2.0 bar Kr) in the upper panel and the corresponing retrieved trace in the lower panel. Reconstructed phase (orange) and intensity (purple) are shown on the right, with the FWHM corresponding to a 19 fs pulse.

The left panel of Fig. 2 shows an SD-FROG trace for a traditional scanning FROG with 2.0 bar of krypton in the S-HCF. The spectrally-resolved SD signal is collected as the temporal delay between the two pulse replicas is scanned using a computer-controlled stage. We take advantage of the pulse

[1] In measurements carried out at higher repetition rates, we found that the spectral bandwidth and efficiency were constant (to within 5%) up to 10 kHz. However, the pulses coming out of the fiber showed much more temporal structure when working with Kr gas at repetition rates above 2 kHz. We suspect this is a result of plasma formation due to three-photon ionization in Kr, with plasma recombination not completing before the next pulse in the train at repetition rates above 2-kHz. This is the subject of further investigation.

shaper to compensate for dispersion and minimize the pulse duration by applying a frequency-dependent phase mask ($M(\omega)$) onto the electric field of the pulse ($E(\omega)$) using the AOM ($E'(\omega) = M(\omega)E(\omega)$). For dispersion compensation we use a mask of the form:

$$M(\omega) = e^{i[\frac{\mathrm{GDD}}{2!}(\omega-\omega_0)^2+\frac{\mathrm{TOD}}{3!}(\omega-\omega_0)^3+...]} \quad \textbf{(1)}$$

which follows a typical Taylor series expansion of the phase about a central frequency (ω_0) with second order dispersion (GDD) and third order dispersion (TOD) coefficients. The right panel of Fig. 2 shows the reconstructed $I(t)$ for the pulse, with a FWHM duration of 19 fs (the spectral bandwidth is sufficient to support a 19 fs transform-limited pulse). We use Femtosoft Technology's software to reconstruct our FROG traces. The grid size used was 1024 and the FROG error was 0.006%.

To generate a d-scan, one could continue to use the amplitude-splitting approach in an interferometer and scan the dispersion with the pulse shaper. However, finding exact time-zero in an interferometer is tedious, so we use the spatial mask to split the pulse. This wavefront-splitting technique inherently preserves temporal overlap. In panel (b) of Fig. 1, we spectrally resolve the SD signal from the nonlinear medium as a function of dispersion. The transform-limited pulse duration for this SD d-scan is 20 fs, and the d-scan reconstructs to 22 fs. An SD d-scan provides basic information about the GDD of the pulse, but it is challenging to visually interpret higher order dispersion, compared to an SD-FROG [28]. Therefore, we use the d-scan as a starting point to obtain the GDD needed to compress the pulse, then adjust the TOD and do a final measurement with the scanning FROG.

The FROG characterization technique can also be used with the spatial mask approach. The pulse shaper can create pulse-pairs with controllable delay, mimicking a mechanical delay stage but with automatic alignment and phase stability for a collinear-FROG (C-FROG) [29] measurement. The acoustic mask function (Eq. 2) is applied in the Fourier frequency domain and results in a pair of pulses in the time domain:

$$M(\omega) = A_1 + A_2 e^{-i\omega\tau+i\phi}, \quad \textbf{(2)}$$

where the pulse delay τ, relative amplitudes A_i, and relative phase ϕ are controlled with the pulse shaper (see "4-f AOM Pulse Shaper" inset of Fig. 1). C-FROG traces are challenging to reconstruct because the signal is comprised of four beams: a pair of double pulses made with the pulse shaper that are then split with the spatial mask. Since it is easy to switch between programming a d-scan or a C-FROG with the pulse shaper, we use this technique to corroborate the d-scan with an approximate pulse duration.

Along with automatic pulse compression and characterization, a notable strength of AOM-based pulse shapers is the ability to arbitrarily shape the pulses in amplitude and phase for use in pulse-shape spectroscopy experiments [19, 30]. For example, the same phase mask used for a C-FROG can also be used to generate pulse-pairs for time resolved spectroscopy measurements. The current implementation allows for a maximum of $\sim$ 1 ps delay between the two pulses. To demonstrate such a "double-pulse", Fig. 3 shows scanning SD-FROG traces of a phase-locked pulse pair with 100 fs delay and zero relative phase (top) and π relative phase (bottom) between the two pulses. The spectrally integrated signal (marginal in time) for each trace is plotted on the right, with an integration performed over the spectral axis. Generating such a pulse pair with a traditional interferometer is difficult to do with high phase stability and cannot offer independent control over phase and delay.

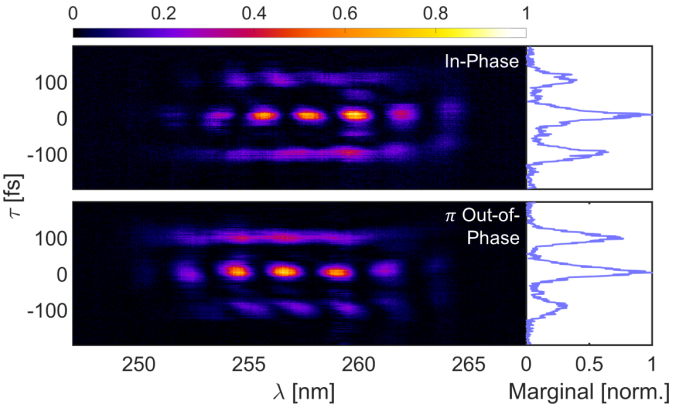

Fig. 3. Scanning SD-FROG traces of equal-amplitude double-pulses at 100 fs delay with zero phase (upper panel) and π phase (lower panel) between the two pulses. The right side shows signal integrated over spectrum for each FROG trace.

The fact that the two pulses share a common optical path means that there is excellent temporal and phase stability between the pulses. To highlight this stability, we include a molecular ionization pump-probe measurement using a double-pulse generated from the pulse shaper (i.e., the first pulse serves as the pump and the second pulse as the probe) [25, 31]. The pump and probe pulses are sent into a vacuum chamber that is injected with a gas-phase molecular sample. For each delay between the pump and the probe, the time-of-flight mass spectrum of the ionization yield is measured with multi-channel plates [32]. Panel (a) of Fig. 4 shows the ionization yield of benzene as a function of pump-probe delay.

There are two pathways to ionization in this measurement, either by one or two probe photons, which are shown in panel (b) of Fig. 4. In the first pathway ("1+1"), the pump pulse excites the molecule to an excited electronic state, and the probe ionizes the excited state. In the other pathway ("0+2"), the probe ionizes the molecule from the ground electronic state with two photons. The 856 as oscillation in Fig. 4 is due to the interference between the two ionization pathways and is a measure of modulations in the electronic density. This oscillation period corresponds to the inverse of the energy separation between the $^1A_{1g}$ ground and $^1B_{2u}$ excited electronic states [33, 34], noted in panel (b) of Fig. 4.

Note that even though the pulses themselves are 20 fs in duration, the excellent temporal/phase stability between the two pulses allows us to resolve sub-femtosecond dynamics. The upper panel shows a scan covering 5 fs of delay using 20 as steps. We can zoom in even further in time and take single attosecond steps (lower panel), where the electronic oscillation period is still easily resolved. Based on this scan, we estimate a temporal stability between the pulse-pair of approximately 6 as, which was calculated by finding the difference in standard deviation of the yield at the maximum and minimum slopes. This stability is ideal for electronic and/or 2D spectroscopy experiments in the DUV.

In conclusion, we demonstrate the generation and shaping of $\sim$ 20 fs pulses in the DUV. We broaden the spectrum after generation of the fourth harmonic of a ytterbium laser and can shape the pulses with our AOM-based pulse shaper. Our pulse shaper can characterize pulses with two methods, a scanning

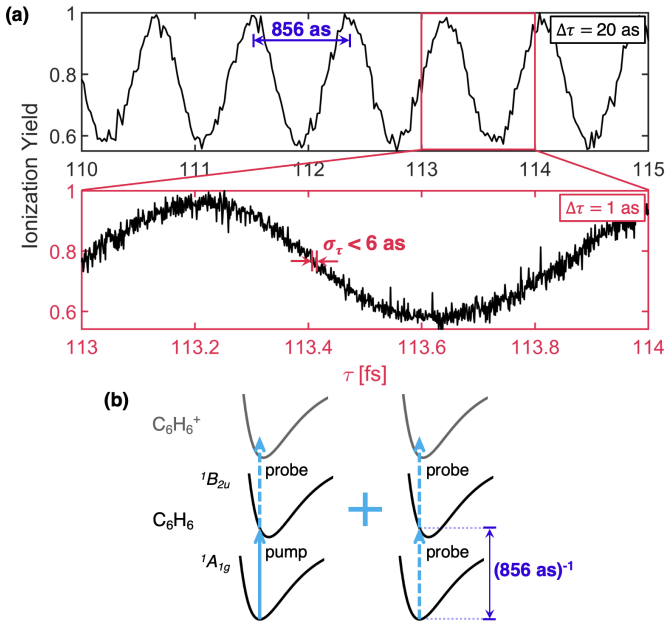

Fig. 4. Panel (a): Double-pulse phase stability measurement showing a benzene ionization signal as a function of delay for a pair of 20 fs pulses. Upper panel: Scan over 5 fs delay using 20 as steps. Lower panel: Scan over 1 fs delay using 1 as steps. **Panel (b):** Ionization pathways "1+1" (left) and "0+2" (right) that produce the measurements in panel (a).

interferometer and a spatial mask, both of which can take d-scan (Fig. 1) and FROG (Fig. 3) measurements. The stability of the shaping capabilities is illustrated with experimental ionization yield data that gives an upper limit to the double pulse timing uncertainty of 6 as. Our compression, shaping and measurement can be carried out without working in vacuum, which allows for flexible and efficient delivery to a variety of different experimental end stations. We are currently implementing the shaped pulses in molecular coherence experiments that take advantage of the pulse energy, shaping, and stability offered by our apparatus.

Funding. B.K and M.B. were funded by the Linac Coherent Light Source, SLAC National Accelerator Laboratory, which is supported by the U.S. Department of Energy, Office of Science, Office of Basic Energy Sciences, under Contract No. DE-AC02-76SF00515. R.F. was supported by the U.S. Department of Energy, Office of Science, Office of Basic Energy Sciences Award No. DE-SC0026078. J.C., L.T.H.N., M.G.C. and T.W. were supported by the National Science Foundation under award number 2409596.

Acknowledgment. The authors thank Joseph Robinson (SLAC National Accelerator Laboratory) for useful discussions.

Disclosures. The authors declare no conflicts of interest.

Data Availability Statement. Data underlying the results presented in this paper are not publicly available at this time but may be obtained from the authors upon reasonable request.

REFERENCES

1. J. P. Lee, T. Avni, O. Alexander, *et al.*, Optica **11**, 1320 (2024).
2. F. Calegari, D. Ayuso, A. Trabattoni, *et al.*, Science **346**, 336 (2014).
3. V. Loriot, A. Boyer, S. Nandi, *et al.*, Nat. Phys. **20**, 765 (2024).
4. C. Homann, P. Lang, and E. Riedle, J. Opt. Soc. Am. B **29**, 2765 (2012).
5. T. Nagy and P. Simon, Opt. letters **34**, 2300 (2009).
6. V. Hariton, Y. Jiang, A. Schönberg, *et al.*, Opt. Lett. **49**, 3769 (2024).
7. P. Baum, S. Lochbrunner, and E. Riedle, Opt. letters **29**, 1686 (2004).
8. B. Schenkel, J. Biegert, U. Keller, *et al.*, Opt. Lett. **28**, 1987 (2003).
9. K. Yamane, Z. Zhang, K. Oka, *et al.*, Opt. Lett. **28**, 2258 (2003).
10. E. Matsubara, K. Yamane, T. Sekikawa, and M. Yamashita, J. Opt. Soc. Am. B **24**, 985 (2007).
11. C. G. Durfee, S. Backus, H. C. Kapteyn, and M. M. Murnane, Opt. Lett. **24**, 697 (1999).
12. J. C. Travers, T. F. Grigorova, C. Brahms, and F. Belli, Nat. Photonics **13**, 547 (2019).
13. V. Wanie, P. Barbato, J. Hahne, *et al.*, J. Physics: Photonics **6**, 025005 (2024).
14. M. Reduzzi, M. Pini, L. Mai, *et al.*, Opt. Express **31**, 26854 (2023).
15. N. Kotsina, C. Brahms, S. L. Jackson, *et al.*, Chem. Sci. **13**, 9586 (2022).
16. A. Catanese, B. Kaufman, C. Cheng, *et al.*, OSA Continuum **4**, 3176 (2021).
17. J. Codere, M. Belmonte, B. Kaufman, *et al.*, Opt. Continuum **3**, 785 (2024).
18. K. L. M. Lewis and J. P. Ogilvie, The J. Phys. Chem. Lett. **3**, 503 (2012).
19. S.-H. Shima and M. T. Zanni, Phys. Chem. Chem. Phys. **11**, 964 (2009).
20. M. A. Dugan, J. X. Tull, and W. S. Warren, J. Opt. Soc. Am. B **14**, 2348 (1997).
21. A. M. Weiner, Opt. Commun. **284**, 3669 (2011). Special Issue on Optical Pulse Shaping, Arbitrary Waveform Generation, and Pulse Characterization.
22. B. J. Pearson and T. C. Weinacht, Opt. Express **15**, 4385 (2007).
23. J. E. H. Young and S.-K. Yao, Proc. IEEE **69**, 54 (1981).
24. E. Eva and K. Mann, Appl. Phys. A **62**, 143 (1996).
25. L. T.-H. Ngo, J. Codere, B. J. Pearson, *et al.*, In Prep. (2025).
26. M. Miranda, C. L. Arnold, T. Fordell, *et al.*, Opt. express **20**, 18732 (2012).
27. M. Canhota, F. Silva, R. Weigand, and H. M. Crespo, Opt. Lett. **42**, 3048 (2017).
28. R. Trebino, K. W. DeLong, D. N. Fittinghoff, *et al.*, Rev. Sci. Inst. **68**, 3277 (1997).
29. I. Amat-Roldán, I. G. Cormack, P. Loza-Alvarez, *et al.*, Opt. Express **12**, 1169 (2004).
30. C.-h. Tseng, S. Matsika, and T. C. Weinacht, Opt. express **17**, 18788 (2009).
31. A. González-Castrillo, F. Martín, and A. Palacios, Sci. reports **10**, 12981 (2020).
32. T. Weinacht and B. J. Pearson, *Time-Resolved Spectroscopy: An Experimental Perspective* (CRC Press, 2018).
33. G. Herzberg, *Molecular Spectra and Molecular Structure. Volume III: Electronic Spectra and Electronic Structure of Polyatomic Molecules*, vol. 3 of *Molecular Spectra and Molecular Structure* (Van Nostrand Reinhold, New York, 1966).
34. E. Pantos, J. Philis, and A. Bolovinos, J. Mol. Spectrosc. **72**, 36 (1978).

FULL REFERENCES

1. J. P. Lee, T. Avni, O. Alexander, *et al.*, "Few-femtosecond soft x-ray transient absorption spectroscopy with tuneable duv-vis pump pulses," Optica **11**, 1320–1323 (2024).
2. F. Calegari, D. Ayuso, A. Trabattoni, *et al.*, "Ultrafast electron dynamics in phenylalanine initiated by attosecond pulses," Science **346**, 336–339 (2014).
3. V. Loriot, A. Boyer, S. Nandi, *et al.*, "Attosecond metrology of the two-dimensional charge distribution in molecules," Nat. Phys. **20**, 765–769 (2024).
4. C. Homann, P. Lang, and E. Riedle, "Generation of 30 fs pulses tunable from 189 to 240 nm with an all-solid-state setup," J. Opt. Soc. Am. B **29**, 2765–2769 (2012).
5. T. Nagy and P. Simon, "Generation of 200-μj, sub-25-fs deep-uv pulses using a noble-gas-filled hollow fiber," Opt. letters **34**, 2300–2302 (2009).
6. V. Hariton, Y. Jiang, A. Schönberg, *et al.*, "Uv 30 fs laser pulse generation using a multi-pass cell," Opt. Lett. **49**, 3769–3772 (2024).
7. P. Baum, S. Lochbrunner, and E. Riedle, "Tunable sub-10-fs ultraviolet pulses generated by achromatic frequency doubling," Opt. letters **29**, 1686–1688 (2004).
8. B. Schenkel, J. Biegert, U. Keller, *et al.*, "Generation of 3.8-fs pulses from adaptive compression of a cascaded hollow fiber supercontinuum," Opt. Lett. **28**, 1987–1989 (2003).
9. K. Yamane, Z. Zhang, K. Oka, *et al.*, "Optical pulse compression to 3.4fs in the monocycle region by feedback phase compensation," Opt. Lett. **28**, 2258–2260 (2003).
10. E. Matsubara, K. Yamane, T. Sekikawa, and M. Yamashita, "Generation of 2.6 fs optical pulses using induced-phase modulation in a gas-filled hollow fiber," J. Opt. Soc. Am. B **24**, 985–989 (2007).
11. C. G. Durfee, S. Backus, H. C. Kapteyn, and M. M. Murnane, "Intense 8-fs pulse generation in the deep ultraviolet," Opt. Lett. **24**, 697–699 (1999).
12. J. C. Travers, T. F. Grigorova, C. Brahms, and F. Belli, "High-energy pulse self-compression and ultraviolet generation through soliton dynamics in hollow capillary fibres," Nat. Photonics **13**, 547–554 (2019).
13. V. Wanie, P. Barbato, J. Hahne, *et al.*, "Ultraviolet supercontinuum generation using a differentially-pumped integrated glass chip," J. Physics: Photonics **6**, 025005 (2024).
14. M. Reduzzi, M. Pini, L. Mai, *et al.*, "Direct temporal characterization of sub-3-fs deep uv pulses generated by resonant dispersive wave emission," Opt. Express **31**, 26854–26864 (2023).
15. N. Kotsina, C. Brahms, S. L. Jackson, *et al.*, "Spectroscopic application of few-femtosecond deep-ultraviolet laser pulses from resonant dispersive wave emission in a hollow capillary fibre," Chem. Sci. **13**, 9586–9594 (2022).
16. A. Catanese, B. Kaufman, C. Cheng, *et al.*, "Acousto-optic modulator pulse-shaper compression of octave-spanning pulses from a stretched hollow-core fiber," OSA Continuum **4**, 3176–3183 (2021).
17. J. Codere, M. Belmonte, B. Kaufman, *et al.*, "High repetition-rate pulse shaping of a spectrally broadened yb femtosecond laser," Opt. Continuum **3**, 785–794 (2024).
18. K. L. M. Lewis and J. P. Ogilvie, "Probing photosynthetic energy and charge transfer with two-dimensional electronic spectroscopy," The J. Phys. Chem. Lett. **3**, 503–510 (2012).
19. S.-H. Shima and M. T. Zanni, "How to turn your pump–probe instrument into a multidimensional spectrometer: 2d ir and vis spectroscopies via pulse shaping," Phys. Chem. Chem. Phys. **11**, 964–980 (2009).
20. M. A. Dugan, J. X. Tull, and W. S. Warren, "High-resolution acousto-optic shaping of unamplified and amplified femtosecond laser pulses," J. Opt. Soc. Am. B **14**, 2348–2358 (1997).
21. A. M. Weiner, "Ultrafast optical pulse shaping: A tutorial review," Opt. Commun. **284**, 3669–3692 (2011). Special Issue on Optical Pulse Shaping, Arbitrary Waveform Generation, and Pulse Characterization.
22. B. J. Pearson and T. C. Weinacht, "Shaped ultrafast laser pulses in the deep ultraviolet," Opt. Express **15**, 4385–4388 (2007).
23. J. E. H. Young and S.-K. Yao, "Design considerations for acousto-optic devices," Proc. IEEE **69**, 54–64 (1981).
24. E. Eva and K. Mann, "Calorimetric measurement of two-photon absorption and color-center formation in ultraviolet-window materials," Appl. Phys. A **62**, 143–149 (1996).
25. L. T.-H. Ngo, J. Codere, B. J. Pearson, *et al.*, In Prep. (2025).
26. M. Miranda, C. L. Arnold, T. Fordell, *et al.*, "Characterization of broadband few-cycle laser pulses with the d-scan technique," Opt. express **20**, 18732–18743 (2012).
27. M. Canhota, F. Silva, R. Weigand, and H. M. Crespo, "Inline self-diffraction dispersion-scan of over octave-spanning pulses in the single-cycle regime," Opt. Lett. **42**, 3048–3051 (2017).
28. R. Trebino, K. W. DeLong, D. N. Fittinghoff, *et al.*, "Measuring ultrashort laser pulses in the time-frequency domain using frequency-resolved optical gating," Rev. Sci. Inst. **68**, 3277–3295 (1997).
29. I. Amat-Roldán, I. G. Cormack, P. Loza-Alvarez, *et al.*, "Ultrashort pulse characterisation with SHG collinear-FROG," Opt. Express **12**, 1169–1178 (2004).
30. C.-h. Tseng, S. Matsika, and T. C. Weinacht, "Two-dimensional ultrafast fourier transform spectroscopy in the deep ultraviolet," Opt. express **17**, 18788–18793 (2009).
31. A. González-Castrillo, F. Martín, and A. Palacios, "Quantum state holography to reconstruct the molecular wave packet using an attosecond xuv–xuv pump-probe technique," Sci. reports **10**, 12981 (2020).
32. T. Weinacht and B. J. Pearson, *Time-Resolved Spectroscopy: An Experimental Perspective* (CRC Press, 2018).
33. G. Herzberg, *Molecular Spectra and Molecular Structure. Volume III: Electronic Spectra and Electronic Structure of Polyatomic Molecules*, vol. 3 of *Molecular Spectra and Molecular Structure* (Van Nostrand Reinhold, New York, 1966).
34. E. Pantos, J. Philis, and A. Bolovinos, "The extinction coefficient of benzene vapor in the region 4.6 to 36 eV," J. Mol. Spectrosc. **72**, 36–43 (1978).